

End Point of a First-Order Phase Transition in Many-Flavor Lattice QCD at Finite Temperature and Density

Shinji Ejiri¹ and Norikazu Yamada^{2,3}

¹ Graduate School of Science and Technology, Niigata University, Niigata 950-2181, Japan

² KEK Theory Center, Institute of Particle and Nuclear Studies,

High Energy Accelerator Research Organization (KEK), Tsukuba 305-0801, Japan

³ School of High Energy Accelerator Science, The Graduate

University for Advanced Studies (Sokendai), Tsukuba 305-0801, Japan

(Dated: March 30, 2013)

Towards the feasibility study of the electroweak baryogenesis in realistic technicolor scenario, we investigate the phase structure of $(2 + N_f)$ -flavor QCD, where the mass of two flavors is fixed to a small value and the others are heavy. For the baryogenesis, an appearance of a first order phase transition at finite temperature is a necessary condition. Using a set of configurations of two-flavor lattice QCD and applying the reweighting method, the effective potential defined by the probability distribution function of the plaquette is calculated in the presence of additional many heavy flavors. Through the shape of the effective potential, we determine the critical mass of heavy flavors separating the first order and crossover regions and find it to become larger with N_f . We moreover study the critical line at finite density and the first order region is found to become wider as increasing the chemical potential. Possible applications to real $(2 + 1)$ -flavor QCD are discussed.

PACS numbers: 11.15.Ha, 12.38.Gc, 12.38.Mh, 12.60.Nz

Introduction. Precise knowledge of the phase structure of finite temperature QCD could offer an opportunity to probe the physics beyond the standard model (SM), provided that new gauge theory induces dynamical electroweak (EW) symmetry breaking. Technicolor (TC) is such a model [1], where the Higgs sector in the SM is replaced by a new strongly interacting gauge theory and its spontaneous chiral symmetry breaking ($S\chi SB$) causes EW symmetry breaking. TC is a vectorlike gauge theory, and if we choose $SU(3)$ as a gauge group it is essentially QCD. The difference is only in their dynamical scales: ~ 1 TeV for TC and ~ 1 GeV for QCD. Thus, numerical techniques developed in lattice QCD trivially apply to the study of TC, where the lattice cutoff is determined by equating the pion decay constant to 246 GeV (Higgs vacuum expectation value). The realizability of this model is now actively investigated using lattice gauge theory [2]. We consider TC including many fermion flavors transforming as the fundamental representation of $SU(3)$ since the presence of many flavors potentially resolves various problems in classical TC.

In this work, we focus on the possibility of the EW baryogenesis within the TC scenario [3], which requires TC gauge theories to go through a strong first order chiral phase transition. The nature of the phase transition depends on the number of flavors and masses [4]. In realistic TC models, two flavors of them are exactly massless and the resulting three massless Nambu-Goldstone (NG) bosons are absorbed into the longitudinal mode of the weak gauge bosons. On the other hand, the mass of other N_f flavors must be larger than an appropriate lower bound otherwise $S\chi SB$ produces too many (light pseudo) NG bosons, none of which is observed yet. Consulting

the study of $(2+1)$ -flavor QCD including up, down and massive strange quarks, the first order transition is realized when the strange mass is below the critical mass. Thus, requiring the first order EW phase transition in TC model brings in the upper bound on the mass of N_f flavors. This motivates us to study the thermal nature of $(2 + N_f)$ -flavor QCD. As discussed below, the critical mass increases with N_f . Hence, the boundary of the first order region can be investigated more easily for large N_f .

Another purpose of this study is to understand the real QCD with $2+1$ flavors. At the physical masses and zero density, the chiral transition is crossover, and is expected to become first order at a critical density. The determination of the critical density is one of the most interesting topics in the study of QCD. To this end, finding the critical surface in the masses and chemical potential parameter space is important [5, 6]. However, recent lattice QCD studies suggest that the critical region at zero density is accessible only when the quark masses are very small and thus its determination is difficult [7]. The study of many-flavor QCD is a good testing ground for investigating N_f -independent universal properties, such as the critical scaling near the tricritical point, which is expected in the up down quark massless limit. This will provide important information for $(2 + 1)$ -flavor QCD.

Method. To study the phase transition, we calculate the effective potential defined by the probability distribution function of the plaquette. The distribution function has two peaks at a first order transition, since two phases coexist with the same probability. The nature of the transition can be thus identified through the shape of the potential [8, 9]. We define the plaquette distribution function for $(2 + N_f)$ -flavor QCD with the quark masses

m_f and chemical potential μ_f ($f = 1, \dots, N_f + 2$) by

$$w(P; \beta, m_f, \mu_f) = \int \mathcal{D}U \mathcal{D}\psi \mathcal{D}\bar{\psi} \delta(P - \hat{P}) e^{-S_g - S_q} \\ = \int \mathcal{D}U \delta(P - \hat{P}) e^{6\beta N_{\text{site}} \hat{P}} \prod_{f=1}^{N_f+2} (\det M(m_f, \mu_f)), \quad (1)$$

where S_g and S_q are the gauge and quark actions, respectively, and M is the quark matrix. $N_{\text{site}} \equiv N_s^3 \times N_t$ is the number of sites. $\beta = 6/g_0^2$ is the lattice bare parameter. \hat{P} is the generalized plaquette operator, and this method is applicable to the case of improved actions replacing \hat{P} to $\hat{P} = -S_g/(6N_{\text{site}}\beta)$. Normalizing by the partition function, $\mathcal{Z} = \int w(P) dP$, eq. (1) gives the histogram for \hat{P} . The effective potential is then given by

$$V_{\text{eff}}(P; \beta, m_f, \mu_f) = -\ln w(P; \beta, m_f, \mu_f). \quad (2)$$

We consider QCD with two degenerate light quarks of the mass m_l and the chemical potential μ and N_f heavy quarks. Denoting the potential of two-flavor QCD at $\mu=0$ by $V_0(P; \beta)$, that of $(2 + N_f)$ -flavor QCD is written as

$$V_{\text{eff}}(P; \beta, m_f, \mu) = V_0(P; \beta_0) - \ln R(P; \beta, m_f, \mu; \beta_0), \quad (3)$$

with

$$\ln R(P; \beta, m_f, \mu; \beta_0) = 6(\beta - \beta_0) N_{\text{site}} P \\ + \ln \left\langle \left(\frac{\det M(m_l, \mu)}{\det M(m_l, 0)} \right)^2 \prod_{f=1}^{N_f} \frac{\det M(m_f, \mu_f)}{\det M(\infty, 0)} \right\rangle_{P:\text{fixed}}, \quad (4)$$

where $\langle \dots \rangle_{P:\text{fixed}} \equiv \langle \delta(P - \hat{P}) \dots \rangle_{\beta_0} / \langle \delta(P - \hat{P}) \rangle_{\beta_0}$ and $\langle \dots \rangle_{\beta_0}$ denotes the ensemble average over two-flavor configurations generated at β_0 , m_l , and vanishing μ . Since the m_l dependence is not discussed in the following, m_l is omitted from the arguments. β_0 is the simulation point, which may differ from β in this method. By performing simulations at various β_0 , one can obtain the potential in a wide range of P .

Restricting the calculation to the heavy quark region, the second determinant for N_f flavors in eq. (4) is approximated by the leading order as

$$\ln \left[\frac{\det M(\kappa_h)}{\det M(0)} \right] = 288 N_{\text{site}} \kappa_h^4 \hat{P} + 12 N_s^3 (2\kappa_h)^{N_t} \hat{\Omega} + \dots \quad (5)$$

for the standard Wilson quark action and

$$\ln \left[\frac{\det M(m_h)}{\det M(\infty)} \right] = \frac{36 N_{\text{site}}}{(2m_h)^4} \hat{P} + \frac{6 N_s^3}{(2m_h)^{N_t}} \hat{\Omega} + \dots \quad (6)$$

for the four-flavor standard staggered quark with m_h . κ_h in eq. (5) is the hopping parameter being proportional to $1/m_h$, and $\hat{\Omega}$ is the real part of the Polyakov loop $\hat{\Omega}_R$ for $\mu_f = 0$ and $\hat{\Omega} = \cosh(\mu_h/T) \hat{\Omega}_R + i \sinh(\mu_h/T) \hat{\Omega}_I$ for $\mu_f = \mu_h$, including the complex phase from the

imaginary part of the Polyakov loop $\hat{\Omega}_I$. For improved gauge actions such as $S_g = -6N_{\text{site}}\beta[c_0(\text{plaquette}) + c_1(\text{rectangle})]$, additional $c_1 \times O(\kappa^4)$ terms must be contained in eqs. (5) and (6), where c_1 is the improvement coefficient and $c_0 = 1 - 8c_1$. However, since the improvement term does not affect the physics, we will cancel these terms by a shift of the coefficient c_1 .

At a first order transition point, V_{eff} shows a double-well shape as a function of P , and, equivalently, the curvature of the potential d^2V_{eff}/dP^2 takes a negative value in a region of P . To observe this behavior, β must be adjusted to be the first order transition point. However, from eqs. (3) and (4), d^2V_{eff}/dP^2 is independent of β . The fine tuning is not necessary in this case [8]. Moreover, d^2V_{eff}/dP^2 over the wide range of P can be easily obtained by combining data obtained at different β . We therefore focus on the curvature of the effective potential to identify the nature of the phase transition.

Denoting $h = 2N_f(2\kappa_h)^{N_t}$ for N_f degenerate Wilson quarks, or $h = N_f/(4 \times (2m_h)^{N_t})$ for the staggered quarks, we obtain $\ln R(P; \beta, \kappa_h, 0; \beta_0) = \ln \bar{R}(P; h, 0) + (\text{plaquette term}) + O(\kappa_h^{N_t+2})$ for $\mu = \mu_h = 0$ with

$$\bar{R}(P; h, 0) = \left\langle \exp[6hN_s^3\hat{\Omega}] \right\rangle_{P:\text{fixed}, \beta_0}. \quad (7)$$

Notice that $\bar{R}(P; h, 0)$ does not depend on β_0 . The plaquette term does not contribute to d^2V_{eff}/dP^2 and can be absorbed by shifting $\beta \rightarrow \beta^* \equiv \beta + 48N_f\kappa_h^4$ for Wilson quarks. Moreover, one can deal with the case with non-degenerate masses by adopting $h = 2 \sum_{f=1}^{N_f} (2\kappa_f)^{N_t}$ or $h = (1/4) \sum_{f=1}^{N_f} (2m_f)^{-N_t}$. Thus, the choice of the quark action is not important. In the following, we discuss the mass dependence of \bar{R} through the parameter h .

Numerical results. We use the two-flavor QCD configurations generated with p4-improved staggered quark and Symanzik-improved gauge actions in Ref. [10], thus $\hat{P} = -S_g/(6N_{\text{site}}\beta)$. The lattice size N_{site} is $16^3 \times 4$. The data are obtained at sixteen values of β from $\beta = 3.52$ to 4.00 keeping the bare quark mass to $ma = 0.1$. The number of trajectories is 10000 – 40000, depending on β . The corresponding temperature normalized by the pseudo-critical temperature is in the range of $T/T_c = 0.76$ to 1.98, and the pseudo-critical point is about $\beta = 3.65$, where the ratio of pseudo-scalar and vector meson masses is $m_{\text{PS}}/m_{\text{V}} \approx 0.7$. All configurations are used for the analysis at zero density, while the finite density analysis is performed every 10 trajectories. Further details on the simulation parameters are given in Ref. [10]. The same data set is used to study the phase structure of two-flavor QCD at finite density in Ref. [8].

We first calculate the potential in two-flavor QCD at zero density, $V_0(P; \beta)$, the first term in eq. (3). Because the finite temperature transition is crossover for two-flavor QCD at a finite quark mass, the distribution function is always Gaussian type. We thus evaluate the

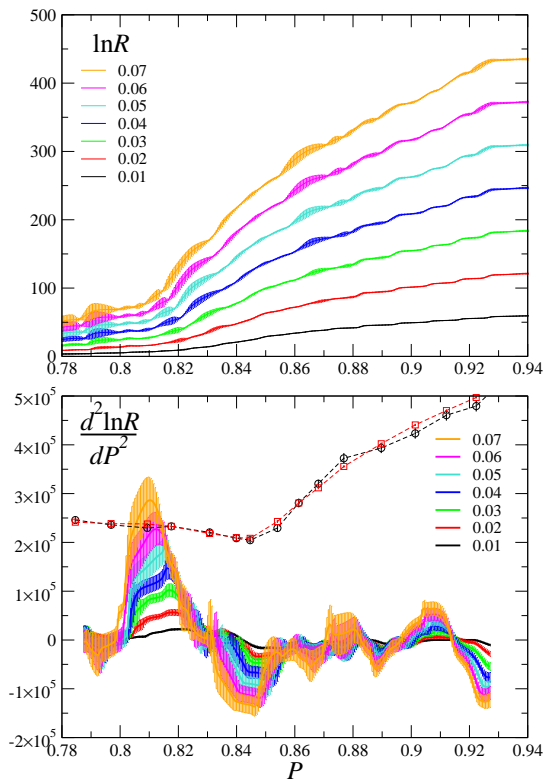


FIG. 1: Top: $\ln \bar{R}(P; h, 0)$ as functions of the plaquette. Bottom: The curvature of $\ln \bar{R}(P; h, 0)$ for $h = 0.01 - 0.07$. The circle and square symbols are $d^2 V_0 / dP^2(P)$.

curvature of V_0 using an identity for the Gaussian distribution, $d^2 V_0 / dP^2 = 6N_{\text{site}} / \chi_P$, where χ_P is the plaquette susceptibility, $\chi_P \equiv 6N_{\text{site}} \langle (P - \langle P \rangle)^2 \rangle$. The slope of V_0 in the heavy quark limit can be also measured using an equation derived from eqs. (3) and (4). When one performs a simulation at β_0 , the slope is zero at the minimum of $V_0(P; \beta_0)$, and the minimum is realized at $P \approx \langle \hat{P} \rangle_{\beta_0}$. Hence, we obtain $dV_0/dP(\langle \hat{P} \rangle_{\beta_0}, \beta) = -6(\beta - \beta_0)N_{\text{site}}$ [11]. The result of $d^2 V_0 / dP^2$ is plotted in the bottom panel of Fig. 1. The circle symbols with dashed lines are calculated by χ_P . The square symbols are computed by the numerical differential of dV_0/dP obtained at the minimum of V_0 . dV_0/dP are the squares in Fig. 2. These results obtained by two different methods are consistent.

Zero density. In the calculation of $\bar{R}(P; h, 0)$, we use the delta function approximated by $\delta(x) \approx 1/(\Delta\sqrt{\pi}) \exp[-(x/\Delta)^2]$, where $\Delta = 0.0025$ is adopted consulting the resolution and the statistical error. Because $\bar{R}(P; h, 0)$ is independent of β , we mix all data obtained at different β as is done in Ref. [8]. The results for $\ln \bar{R}(P; h, 0)$ are shown by solid lines in the top panel of Fig. 1 for $h = 0.01 - 0.07$. A rapid increase is observed around $P \sim 0.82$. It is also important to note that the gradient becomes larger as h increases.

The second derivative $d^2 \ln \bar{R} / dP^2$ is calculated by fitting $\ln \bar{R}$ to a quadratic function of P with a range of

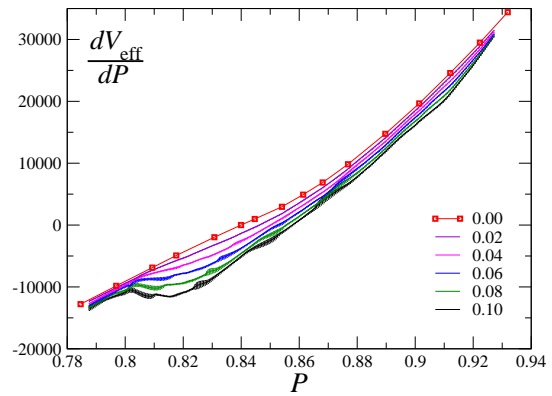


FIG. 2: The slope of $V_{\text{eff}}(P; \beta, h, 0)$ normalized at $(\beta, h) = (3.65, 0)$ for $h = 0.0 - 0.1$. The squares are dV_0/dP .

$P \pm 0.015$ and repeating with various P . The results are plotted in Fig. 1 (bottom), where $d^2 V_0 / dP^2$ is also shown as the circles or the squares with dashed lines. This figure shows that $d^2(\ln \bar{R}) / dP^2$ becomes larger with h , and the maximum around $P = 0.81$ exceeds $d^2 V_0 / dP^2$ for $h > 0.06$. This indicates that the curvature of the effective potential, $d^2 V_{\text{eff}} / dP^2 = d^2 V_0 / dP^2 - d^2(\ln \bar{R}) / dP^2$, vanishes at $h \sim 0.06$ and a region of P where the curvature is negative appears for large h . We estimated the critical value h_c at which the minimum of $d^2 V_{\text{eff}} / dP^2$ vanishes and obtained $h_c = 0.0614(69)$.

To see the appearance of the first order transition in a different way, we plot dV_{eff}/dP at finite h for $\beta^* = 3.65$ in Fig. 2. The shape of the dV_{eff}/dP is independent of β because $d^2 V_{\text{eff}} / dP^2$ is β -independent. dV_{eff}/dP is monotonically increasing when h is small, indicating that the transition is crossover. However, the shape of dV_{eff}/dP turns into an S-shaped function at $h \sim 0.06$, corresponding to the double-well potential.

We defined the parameter $h = 2N_f \times (2\kappa_h)^{N_t}$ for the Wilson quark. Then, the critical κ_{hc} corresponding h_c decreases as $\kappa_{hc} = [h_c / (2N_f)]^{1/N_t} / 2$ with N_f , and the truncation error from the higher order terms in κ_h becomes smaller as N_f increases. The application range of the hopping parameter expansion was examined in quenched QCD simulations with $N_t = 4$, by explicitly measuring the size of the next-to-leading order (NLO) terms of the expansion [12]. They found that the NLO contribution becomes comparable to that in the leading order at $\kappa_h \sim 0.18$. Hence, this method may be applicable up to around $\kappa_h \sim 0.1$. For instance, in the case of $N_f = 10$ with $N_t = 4$, κ_{hc} is 0.118.

Nonzero density. Finally, we turn on a chemical potential μ for two light quarks and μ_h for N_f flavors, and discuss the μ dependence of the critical mass. Because the strange chemical potential is small in the heavy-ion collisions, the (2+1)-flavor case with $\mu_h = 0$ corresponds to the experiments. As discussed above, we can investigate the critical region easily for large N_f . $\bar{R}(P; h, \mu)$

is then given by $\langle (\det M(m_1, \mu) / \det M(m_1, 0))^2 \times (\det M(m_h, \mu_h) / \det M(\infty, 0))^{N_f} \rangle_{P: \text{fixed}}$. The quark determinant is computed using the Taylor expansion of $\ln[\det M(m_1, \mu) / \det M(m_1, 0)]$ in terms of μ/T up to $O[(\mu/T)^6]$ and the Gaussian approximation is applied to avoid the sign problem as explained in Ref. [8]. This approximation is valid for small μ . The truncation error has been estimated comparing the results up to $O(\mu^4)$ and $O(\mu^6)$ for $\mu/T \leq 2.5$ and is found to be small [8]. The left panel of Fig. 3 shows the curvatures of V_0 and $\ln \bar{R}(P; h, \mu)$ at $\mu/T = 1$, $\mu_h = 0$. The maximum value of $d^2 \ln \bar{R}(P; h, \mu) / dP^2$ is larger than that at $\mu = 0$. This means the critical h is smaller at finite μ . Figure 3 (right) shows the critical value of h as a function of μ for $\mu_h = 0$ (circles) and $\mu_h = \mu$ (diamonds). In the region above this line, the effective potential has the negative curvature region, indicating the transition is of first order. It is clear that the first order region becomes wider as μ increases. If the same behavior is observed in $(2+1)$ -flavor QCD, this gives the strong evidence for the existence of the critical point at finite density in the real world.

Although this analysis is valid only for large N_f , it gives a frame of reference for the study of critical mass at finite μ . Notice that $\ln \bar{R}(P; h, \mu)$ is given by the sum of $\ln \bar{R}(P; 0, \mu)$ and $\ln \bar{R}(P; h, 0)$ approximately and that the behavior of $\ln \bar{R}(P; h, 0)$ in Fig. 1 is very similar to that of $\ln \bar{R}(P; 0, \mu)$ in Figs. 5 and 7 in Ref. [8]. $\ln \bar{R}(P; 0, \mu)$ is estimated from the quark number susceptibility at small μ and $\ln \bar{R}(P; h, 0)$ is obtained from the Polyakov loop at small κ_h . Both the quark number susceptibility and the Polyakov loop rapidly increase at the same value of P near the transition point, which enhances the curvature of $\ln \bar{R}$. Therefore, the critical h decreases with μ or equivalently the critical μ decreases with h . The same argument is possible for $(2+1)$ -flavor.

Conclusion and outlook. We studied the phase structure of $(2+N_f)$ -flavor QCD to explore the realizability of the EW baryogenesis in technicolor scenario and to understand properties of the finite density QCD. Fixing the mass of two light quarks, we determined the critical mass of the other N_f quarks separating the first order and crossover regions. The critical mass is found to become larger with N_f . Furthermore, the chemical potential dependence of the critical mass is investigated for large N_f , and the critical mass is found to increase with μ .

The next step for the estimation of the baryon number asymmetry in TC scenario is to quantify the strength of the first order phase transition. Another interesting application of our method is to study universal scaling behavior near the tricritical point. If the chiral phase transition in the two flavor massless limit is of second order, the boundary of the first order transition region $m_1^c(m_h)$ is expected to behave as $m_1^c \sim |m_h^{\text{tri}} - m_h|^{5/2}$ in the vicinity of the tricritical point, $(m_1, m_h, \mu) = (0, m_h^{\text{tri}}, 0)$, from the mean field analysis. This power behavior is universal for any N_f . The density dependence is important

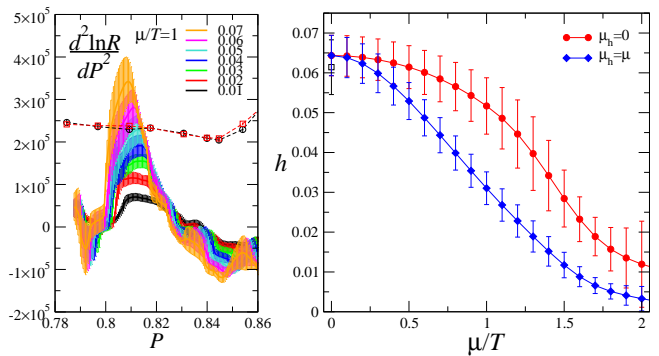


FIG. 3: Left: The curvature of $\ln \bar{R}(P; h, \mu)$ as functions of the plaquette at $\mu/T = 1.0$ and $\mu_h = 0$. Right: The critical line in the (h, μ) plane for $\mu_h = 0$ (circles) and for $\mu_h = \mu$ (diamonds). In the region above this line, the transition is of first order. The square at $\mu = 0$ is computed using all configurations, and the others are measured with every 10.

as well, which is expected to be $m_1^c \sim |\mu|^{5/2}$ [13]. Starting from large N_f , the systematic study of properties of QCD phase transition is possible.

Acknowledgments We would like to thank members of the WHOT-QCD Collaboration for discussions. A part of this work was completed at the GGI workshop. This work is in part supported by Grants-in-Aid of the Japanese Ministry of Education, Culture, Sports, Science and Technology (No. 22740183, 23540295) and by the Grant-in-Aid for Scientific Research on Innovative Areas (No. 20105002, 20105005, 23105706).

-
- [1] S. Weinberg, Phys. Rev. D **13**, 974 (1976); L. Susskind, Phys. Rev. D **20**, 2619 (1979).
 - [2] L. Del Debbio, PoS (**LATTICE 2010**) 004 (2010); K. Rummukainen, AIP Conf. Proc. **1343**, 51 (2011).
 - [3] For semiquantitative analysis on electroweak baryogenesis in the many-flavor TC scenario, see T. Appelquist, M. Schwetz and S. B. Selipsky, Phys. Rev. D **52**, 4741 (1995); Y. Kikukawa, M. Kohda, and J. Yasuda, Phys. Rev. D **77**, 015014 (2008).
 - [4] R. D. Pisarski and F. Wilczek, Phys. Rev. D **29**, 338 (1984).
 - [5] P. de Forcrand and O. Philipsen, Nucl. Phys. B **673**, 170 (2003); JHEP **0701**, 077 (2007).
 - [6] Ch. Schmidt *et al.*, Nucl. Phys. B (Proc. Suppl.) **119**, 517 (2003); F. Karsch *et al.*, Nucl. Phys. B (Proc. Suppl.) **129**, 614 (2004); S. Ejiri *et al.*, Prog. Theor. Phys. Suppl. **153**, 118 (2004).
 - [7] S. Ejiri *et al.*, Phys. Rev. D **80**, 094505 (2009).
 - [8] S. Ejiri, Phys. Rev. D **77**, 014508 (2008).
 - [9] H. Saito *et al.* (WHOT-QCD Collaboration), Phys. Rev. D **84**, 054502 (2011).
 - [10] C. R. Allton *et al.*, Phys. Rev. D **71**, 054508 (2005).
 - [11] S. Ejiri and H. Yoneyama, PoS (**LAT2009**) 173 (2009).
 - [12] WHOT-QCD Collaboration, in preparation.
 - [13] S. Ejiri, PoS (**LATTICE 2008**) 002 (2008).